PROCEEDINGS OF SPIE

SPIEDigitalLibrary.org/conference-proceedings-of-spie

Optimizing channel selection for excitation-scanning hyperspectral imaging

Joshua Deal, Thomas C. Rich, Silas J. Leavesley

Joshua Deal, Thomas C. Rich, Silas J. Leavesley, "Optimizing channel selection for excitation-scanning hyperspectral imaging," Proc. SPIE 10881, Imaging, Manipulation, and Analysis of Biomolecules, Cells, and Tissues XVII, 108811B (4 March 2019); doi: 10.1117/12.2510784



Event: SPIE BiOS, 2019, San Francisco, California, United States

Optimizing channel selection for excitation-scanning hyperspectral imaging

Joshua Deal^{1,2,3}, Thomas C. Rich^{2,3}, Silas J. Leavesley^{1,2,3}
¹Department of Chemical & Biomolecular Engineering, University of South Alabama; ²Center for Lung Biology, University of South Alabama; ³Department of Pharmacology, University of South Alabama;

ABSTRACT

A major benefit of fluorescence microscopy is the now plentiful selection of fluorescent markers. These labels can be chosen to serve complementary functions, such as tracking labeled subcellular molecules near demarcated organelles. However, with the standard 3 or 4 emission channels, multiple label detection is restricted to segregated regions of the electromagnetic spectrum, as in RGB coloring. Hyperspectral imaging allows the user to discern many fluorescence labels by their unique spectral properties, provided there is significant differentiation of their emission spectra. The cost of this technique is often an increase in gain or exposure time to accommodate the signal reduction from separating the signal into many discrete excitation or emission channels. Recent advances in hyperspectral imaging have allowed the acquisition of more signal in a shorter time period by scanning the excitation spectra of fluorophores. Here, we explore the selection of optimal channels for both significant signal separation and sufficient signal detection using excitation-scanning hyperspectral imaging.

Excitation spectra were obtained using a custom inverted microscope (TE-2000, Nikon Instruments) with a Xe arc lamp and thin film tunable filter array (VersaChrome, Semrock, Inc.) Tunable filters had bandwidths between 13 and 17 nm. Scans utilized excitation wavelengths between 340 nm and 550 nm. Hyperspectral image stacks were generated and analyzed using ENVI and custom MATLAB scripts. Among channel consideration criteria were: number of channels, spectral range of scan, spacing of center wavelengths, and acquisition time.

Keywords: Hyperspectral, Fluorescence, Spectroscopy, Microscopy, Signature, Linear Spectral Unmixing, Excitation, Optimization

1. INTRODUCTION

The increasing availability of fluorescent dyes, proteins, and other labels make it possible to label virtually any aspect of a cell with a wide range of the electromagnetic spectrum.¹⁻³ The wide variety of these labels allow for simultaneous labeling of many different aspects of cells, such as a different label per organelle, and can even be used to investigate protein-protein interactions via the properties of Förster resonance energy transfer (FRET) that require very small distances (1-10 nm) for energy transfer to occur.^{4,5} A major limitation to using combinations of several of these fluorescent markers in a single experiment is that it can be difficult to separate the fluorescence signal due to each fluorophore if their emission spectra are not significantly different. To solve this problem, many improvements have been made to the labels themselves and techniques have been investigated which allow separation of these signals with unmixing techniques rather than simply filtering emitted light into discrete channels.^{3,4,6-17} These unmixing techniques work by using the known spectral properties of the fluorescent markers and creating combinations of those markers per pixel to determine the relative contribution of each marker in each pixel. Efforts have been made to determine configurations of imaging parameters to achieve optimal fluorescence signal separation, but most of these efforts concern systems which work by either filtering both excitation and emission light in narrow bands or by tracking fluorescence lifetime.¹⁸

We have recently developed a new hyperspectral imaging approach which scans the excitation spectrum of fluorophores and collects emitted light in very large bands (350+ nm), allowing a much faster scanning speed and higher signal-to-noise ratio. Here, we examine the effects of the number of channels, spectral range of scanning, and spacing of center wavelengths on the spectrally unmixed data taken from cells labeled with at least 4 distinct fluorescent markers. We evaluated using spectral data provided by the manufacturer versus obtaining a spectral library from the data

Imaging, Manipulation, and Analysis of Biomolecules, Cells, and Tissues XVII, edited by Daniel L. Farkas, Attila Tarnok, James F. Leary, Proc. of SPIE Vol. 10881, 108811B · © 2019 SPIE · CCC code: 1605-7422/19/\$18 · doi: 10.1117/12.2510784

acquisition system itself for use in unmixing. Additionally, we compared simple RGB coloring to unmixed component false coloring. Finally, we evaluated channel selection by subsampling each spectral scan originally taken every 5 nm at 10, 15, 20, 25, and 40 nm increments, as well as choosing only the excitation wavelengths that correspond to the peak excitation wavelength of each label. Initial results suggest that surprisingly few excitation wavelengths are necessary to achieve unmixing results similar to results generated from an oversampled dataset.

2. METHODS

2.1 Cell Preparation

Human embryonic kidney 293 (HEK-293) cell culture was performed as described previously. ²⁰⁻²² Briefly, HEK-293 cells were maintained in 10 mL of Minimal Essential Medium (MEM, Life Technologies Inc., Grand Island, NY) containing 10% (vol/vol) fetal bovine serum (Sigma), 100 U/ml penicillin, and 100 μg/ml streptomycin, pH 7.0. Cells were grown in 100 mm culture dishes at 37° C in a humidified atmosphere of 95% air, 5% CO₂. Confluent monolayers were passaged using phosphate-buffered saline containing 0.03% EDTA. Cells were seeded onto 25 mm laminin-coated round glass coverslips and were grown to 70-80% confluency (about 48 h). Prior to imaging, cells were transferred to Attofluor holders (Thermo Fisher Scientific) and covered with 1 ml of extracellular buffer solution containing 145 mM NaCl, 4 mM KCl, 20 mM HEPES, 10 mM D-glucose, 1 mM MgCl₂, and 1 mM CaCl₂, at pH 7.3.

2.2 Excitation-scanning microscope setup and image acquisition

All imaging was performed on an inverted fluorescence microscope (TE2000-U, Nikon Instruments, Melville, New York), a 60X objective (Plan Apo VC 60X/1.2 WI ∞ /0.15-0.18 WD 0.27, Nikon Instruments) and Laser-Driven Light Source (EQ-77 LDLS, Energetiq, Woburn, MA) for excitation. Excitation wavelength tuning (340 to 550 nm in 5-nm increments) was achieved via a custom array of five thin-film tunable filters (TBP01-378/16, TBP01-402/16, TBP01-449/15, TBP01-501/15, and TBP01-561/14, Semrock Inc., Rochester, New York) immediately following the excitation source. The tunable filters were mounted in a high-speed tiltable filter-wheel (Lambda VF-5, Sutter Instrument Company). A filter cube consisting of a long-pass emission filter (BLP02 561R-25, Semrock Inc.) and a dichroic beamsplitter (FF555-Di03, Semrock Inc.) was utilized to separate excitation from emission light at 550 nm. Fluorescence images were acquired using a high-sensitivity scientific complementary metal-oxide semiconductor (sCMOS) camera (Prime 95B, Photometrics, Tucson, AZ).

2.3 Image Processing and Analysis

Spectral images were processed into image stacks with a custom MATLAB (MathWorks, Natick, MA) script. Resultant images were visualized with ENVI software (Exelis Visual Information Solutions, Boulder, CO) as three-dimensional image cubes composed of two spatial and one spectral dimension (spectral image cube). Images were false colored in the spectral dimension according to wavelength-dependent intensity. Blue, green, and red false-colorings were applied to the images at 10%, 50%, and 90% of the spectral range, respectively. Background subtraction and wavelength-dependent illumination were completed as described previously. Briefly, a pixel-averaged background spectrum was extracted from regions of the image containing no cells then subtracted from the image stack. Image stacks were then corrected for wavelength-dependent illumination by multiplication of correction coefficients determined by use of a NIST-traceable lamp (LS-1-CAL-INT, Ocean Optics, Inc.) and a fiber-coupled spectrometer (QE65000, Ocean Optics, Inc.) as described previously.²³

2.4 Spectral Libraries

A total of 6 fluorescent labels, all acquired from Thermo Fisher Scientific, were used for this study. The labels were: Tetramethylrhodamine conjugated wheat germ agglutinin (TRITC WGA, W849), Calcein Green AM (C34852), MitoTracker Green FM (M7514), Fura Red AM (F3021), Fura-2 AM (F1221), and NucBlue (R37605). All labels were added to the previously described buffer solution and incubated for 20 minutes, with the exception of WGA which was added 5 minutes prior to rinsing to avoid nonspecific labeling, per manufacturer instructions. Labels were added in the following concentrations: Calcein Green AM, Fura-2 AM, and Fura Red AM at 20 μ M; MitoTracker Green FM at 100 nM; TRITC WGA at 5 μ g/ml; and NucBlue at 3 drops per 1 ml buffer. To generate a spectral library, each label was added alone to a single coverslip of HEK-293 cells to generate a single-label control spectrum.

Additionally, Thermo Fisher Scientific has the spectral information for these dyes available via the Thermo Fisher Scientific Fluorescence SpectraViewer. Data from the SpectraViewer were exported and plotted in 5 nm increments for comparison with the spectral library generated from the single-label controls acquired using the excitation-scanning

microscope. As in the spectral data generation and acquisition described below, the libraries were subsampled to determine efficacy of unmixing with fewer excitation wavelength datapoints.

2.5 Spectral Image Analysis

Spectral images were analyzed with both ENVI software and custom MATLAB scripts. First, the processed hyperspectral image cubes were opened with ENVI software for visualization. Next, a custom MATLAB script utilized non-negatively constrained linear regression for spectral unmixing to generate a fluorescence intensity image per fluorophore in a given library. Any signal not accounted for by spectral unmixing was included as the root-mean-square (RMS) error. The RMS error calculation has been described previously.²⁵

3. RESULTS AND DISCUSSION

A key step when unmixing a spectral data set is to ensure the accuracy of the library. To that end, the excitation spectral data for each label was collected and exported from the Thermo Fisher Scientific Spectra Viewer and pared down to every 5 nm of the spectral range considered in the following experimental scans (Figure 1). For comparison, each individual label was also added alone to a single coverslip containing confluent HEK-293 cells. An additional coverslip was used to collect any autofluorescence data from the HEK-293 cells. No fewer than four fields of view were collected and averaged to generate the spectral library data for each fluorescent label (and autofluorescence). Both spectral libraries are shown in Figure 1. It is worth noting that both Fura-2 and Fura Red have different excitation spectra depending on whether the label is bound or free. The library obtained from the excitation-scanning microscope does not account for these different spectra, opting instead for a single excitation spectrum of each Fura. Furthermore, there is no autofluorescence data available for the HEK-293 cell line through the Thermo Fisher Scientific Spectra Viewer.

There are a few important observations to make about the excitation-scanning library. First, a number of the fluorescent labels with longer excitation peak wavelengths in the Spectra Viewer library (Fura Red, MitoTracker Green, TRITC WGA) were measured to have peaks in the ultraviolet region on the excitation-scanning system. This is potentially an artifact of insignificant background removal which was amplified when the correction factor was applied, as the correction factor adjusts the intensities based on illumination power per wavelength. As this light source produces more intense light in the visible spectrum than the ultraviolet region, it is possible that any background noise in the ultraviolet region not sufficiently removed during background subtraction was scaled up during the correction process. Similarly, there is a peak that appears in each label (including autofluorescence) at 455 nm. This peak also appears to be intensity dependent, as the labels with a higher normalized intensity at that wavelength appear to show a more dramatic increase in that wavelength alone. However, as all of the data obtained throughout this study were processed in the same manner as the library data, it is likely that these same shifts appear in the rest of the datasets and the reported library is therefore appropriate for this study.

A comparison of spectral unmixing with these two libraries as well as a standard RGB false-coloring is shown in Figure 2 (Left Column). The process of RGB false-coloring excitation-scanning hyperspectral images has been described in detail previously. Briefly, the corrected wavelength-dependent intensity images at 10%, 50%, and 90% of the spectral range of the excitation scan were colored blue, green, and red respectively. In the case of a 340 – 550 nm range, these are the 355, 445, and 530 images. The above non-negatively constrained unmixing algorithm was applied to the same set of images using both the excitation-scanning microscope and Spectra Viewer libraries. Each image was linearly scaled for visualization purposes only between the range of minimum and maximum intensity per image and given a false color. The false color images were subsequently merged as a composite image.

Visually, the RGB image leaves much to be desired (Figure 2 – Left Column). The cell nuclei are clearly discernable in the 355 nm image and the cell membranes (labeled with the TRITC WGA) are clearly discernable in the 530 nm image, but every other label is either agglomerated into the 445 nm image or partially contained in the other two wavelength images. The result is a blurry image with fairly well defined nuclear and membrane regions, but little else. The comparison between unmixing libraries gives much more detail. When reporting the data unmixed with the Spectra Viewer library (Figure 2 – Center Column), the images for the "bound" and "free" Fura labels were combined for each respective label. That is, the "Fura-2" and "Fura Red" images from the unmixed data using the Spectra Viewer library are the summed images of the unmixed Fura-2 (Free) + Fura-2 (Bound) and Fura Red (Free) and Fura Red (Bound) images, labeled in Figure 2 as Fura-2 (Total) and Fura Red (Total). Both libraries yielded similar unmixing data for NucBlue, Calcein Green, and TRITC WGA. Coincidentally, these are the three brightest labels present in the sample. However, both the Fura labels and the MitoTracker label show significant differences. Notably, the Fura-2 image

unmixed with the Spectra Viewer library is very similar to the NucBlue image, while unmixing with the library obtained from the excitation-scanning microscope (Figure 2 – Right Column) shows more signal spaced throughout the cytosol. Additionally, the microscope library shows Fura Red in much more concentrated regions whereas the Spectra Viewer library suggests that Fura Red is almost omnipresent. Similarly, the Spectra Viewer library suggests than an unlikely high percentage of pixels contain signal from MitoTracker Green, while the microscope library places those signals in discrete locations near the nuclei; a much more realistic distribution for mitochondria. The composite images are even more telling. Due to the additive nature of light when creating these false-color composite images, a large portion of the Spectra Viewer library composite image appears white, indicating that there is appreciable unmixed signal from virtually every fluorescent label in those pixels. Furthermore, the locations and concentrations of the unmixed signals obtained with the microscope library appear visually more. In either case, the overwhelmingly bright nature of the Calcein Green label, coupled with it being one of three calcium labels present in the experiment, led us to exclude it from future experiments. With these details in consideration, the remaining unmixing will be performed using the excitation-scanning spectral microscope library.

With the proper library for spectral unmixing established, we next sought to investigate an optimal center wavelength spacing to achieve acceptable levels of fluorescent label separation. That is, we subsampled our data set (originally acquired by collecting excitation-scanning data every 5 nm using filters with bandpasses between 13-17 nm) to simulate data acquired every 10, 15, 20 (Figure 3, top row), 25, and 40 nm (Figure 3, middle row) using the same filter set. Additionally, rather than equally spacing the center wavelengths, we simulated an experimental set containing the excitation wavelength images that correspond to the peak excitation wavelength of each fluorescent label (Figure 3, bottom row). In this case, the selected wavelengths were 340 nm (autofluorescence), 345 nm (NucBlue), 370 nm (Fura-2), 455 nm (Fura Red), 475 nm (Fura Red), 500 nm (MitoTracker Green), and 550 nm (TRITC WGA). Due to the nature of spectral unmixing algorithms, the Fura-2 peak was chosen to correspond to the data acquired from the Spectra Viewer library, as the reported microscope library peak is shared with NucBlue, leaving too few datapoints for the unmixing algorithm to work appropriately. That is, there must be as many excitation wavelength images as fluorescent labels when unmixing or the algorithm will report infinitely many best solutions. ^{18,27} Similarly, as the reported Fura Red maximum is the curious peak present at 455 nm, the excitation wavelength with the second-highest intensity (475 nm) was also chosen for inclusion in the "peak wavelength" library to both aid in proper dimensionality and an accurate representation of the Fura Red label.

The results of spectral unmixing with varied spacing between center wavelengths are surprisingly similar (Figure 4). The original spacing of 5 nm was chosen as a set of control unmixed images. As the bandwidths of the spectral filters were between 13-17 nm, the 20 nm distance was chosen to show a data set where the spectral data among center wavelengths constitute nearly the entire range of the chosen excitation spectrum, but no longer satisfy the contiguous definition that hyperspectral imaging requires. The 40 nm distance represented the furthest, equidistant spacing possible while leaving enough datapoints for the unmixing algorithm to function. In other words, the 40 nm distance represents the fewest possible datapoints that still satisfy the experimental conditions. Finally, the "peak wavelength" library was chosen to simulate traditional fluorescence imaging done with specific filter cubes (e.g. TRITC filter cube). The MitoTracker Green, NucBlue, and TRITC WGA label images appear virtually identical when unmixed with each of these libraries. Slight differences are noticeable in the WGA TRITC images near the top where the cells are clustered and the regions of the cells that correspond to the nucleus became a little sparser. Similarly, fewer pixels were identified to have MitoTracker Green signal as the spacing between center wavelengths increased, but the overall images still appear to be similar. However, both Fura labels appear less specific as this distance increases. In particular, the 40 nm and "peak wavelength" spacing images contain more identified pixels in sporadic regions, resulting in a blurry, halo-like effect. Perhaps the most dramatic difference was observed in autofluorescence images. HEK-293 cells were chosen for these experiments because they are believed to contain little (negligible) autofluorescence. Yet, as the center wavelength spacing increased, far more of the pixels were identified to contain autofluorescence. Regardless of the wavelength spacing, the composite images are all very similar, with the exception of the unmixing performed with the "peak wavelengths" library, where several purplish hazes can be seen throughout the image. However, perhaps the most interesting result is seen in the RMS error row. It appear that the reduction in number of datapoints required for proper fitting results in a smaller error term for most pixels in these images as evidenced by the more sporadic and overall less intense images generated from data sets with fewer datapoints. These data suggest that the increase in acquisition speed and potential reduction in photobleaching reduction are worth the small quality sacrifice in unmixed data generated from widely spaced excitation wavelengths.

4. CONCLUSIONS AND FUTURE WORK

Excitation-scanning hyperspectral imaging is still a recent and infrequently adopted technology. However, new applications of this technology are being investigated as the benefits of excitation-scanning become more well-established. 19,25,26,28–34 As with any new technology, its usefulness and potential applications will expand as devices become more optimized. To that end, it will be necessary to determine the optimal imaging parameters for each desired application. An important first step in any sort of experimentation with complex systems is to first identify how the data are to be assessed. Figure 2 shows that a simple RGB coloring may be sufficient for some applications, given careful selection of fluorescent labels. However, taken together, Figures 1 and 2 demonstrate that, while manufacturer data may be very good, the response on any individual system and to diverse experimental conditions may vary. Thus, it is important to, whenever possible, generate a spectral library of single-labeled controls using the same system that will be used for data acquisition. Finally, the data shown here indicate that, while considering only the peak excitation wavelengths as data points for a given data set are not optimal in some applications, acceptable unmixing quality may be achieved by using as few equally spaced excitation wavelengths as number of fluorescent labels in a given experimental system.

There are several aspects of this experiment that we wish to improve upon in the future. First, like Neher's optimization paper for spectral (emission) systems, 18 we would like to determine a quantitative, objective measurement of optimized imaging parameters as opposed to the subjective metric of simply visualizing the unmixed images. Furthermore, some of the data generated from the single-label controls and subsequent data correction show curious, unexpected details in their excitation spectral data, such as peak excitation wavelengths in the UV region for probes known to fluoresce in the visible spectrum and the curious, intensity-dependent peaks at 455 nm. In the future, we will take much more care to eliminate any scaling artifacts caused by either improper background subtraction or correction factor multiplication. Additionally, the concentrations of the labels here did not necessarily equate in terms of total intensity. The Calcein Green and NucBlue labels in particular were much brighter than the rest of the labels. In future experiments, we will run several more control experiments to determine the proper concentrations of each label to achieve a more uniform response from the fluorescent label mixtures. Similarly, the excitation-scanning microscope library considered only Fura-2 and Fura Red as determined from a single experimental condition, whereas these probes have different spectra when they are in calcium bound or unbound states. In the future, we will recollect the spectral data from these probes in calcium-poor and calcium-rich environments to achieve a more accurate spectral library. Finally, these experiments focused primarily on the number of channels and the spacing between them. In the future, we would also like to explore the effects of varied exposure times and alteration of the range of spectral scans.

5. ACKNOWLEDGEMENTS

We would like to acknowledge the Abraham Mitchell Cancer Research fund as well as the American Heart Association grant 18PRE34060163, National Science Foundation grant NSF 1725937, and National Institutes of Health grants P01HL066299, R01HC137030, UL1 TR001417, S10RR027535, and S10OD020149 for supporting this work. We would also like to thank Energetiq Technology, Inc. for allowing us to collect this data as a demonstration of their EQ-77 laser driven light source coupled to an established excitation-scanning spectral imaging system. Drs. Leavesley and Rich also disclose financial interest in a start-up company, SpectraCyte LLC, formed to commercialize spectral imaging technologies.

REFERENCES

- [1] Panchuk-Voloshina, N., Haugland, R.P., Bishop-Stewart, J., Bhalgat, M.K., Millard, P.J., Mao, F., Leung, W.-Y., and Haugland, R.P., "Alexa dyes, a series of new fluorescent dyes that yield exceptionally bright, photostable conjugates," Journal of Histochemistry & Cytochemistry 47(9), 1179–1188 (1999).
- [2] Zhang, J., Campbell, R.E., Ting, A.Y., and Tsien, R.Y., "Creating new fluorescent probes for cell biology," Nature reviews Molecular cell biology 3(12), 906 (2002).
- [3] Li, B., Yu, Q., and Duan, Y., "Fluorescent labels in biosensors for pathogen detection," Critical reviews in biotechnology 35(1), 82–93 (2015).
- [4] Zimmermann, T., Rietdorf, J., Girod, A., Georget, V., and Pepperkok, R., "Spectral imaging and linear un-mixing enables improved FRET efficiency with a novel GFP2–YFP FRET pair," FEBS letters 531(2), 245–249 (2002).
- [5] Sun, Y., Wallrabe, H., Seo, S., and Periasamy, A., "FRET microscopy in 2010: the legacy of Theodor Förster on the 100th anniversary of his birth," Chemphyschem 12(3), 462–474 (2011).
- [6] Tsurui, H., Nishimura, H., Hattori, S., Hirose, S., Okumura, K., and Shirai, T., "Seven-color fluorescence imaging of tissue samples based on Fourier spectroscopy and singular value decomposition," Journal of Histochemistry & Cytochemistry 48(5), 653–662 (2000).
- [7] Schröck, E., Du Manoir, S., Veldman, T., Schoell, B., Wienberg, J., Ferguson-Smith, M., Ning, Y., Ledbetter, D., Bar-Am, I., et al., "Multicolor spectral karyotyping of human chromosomes," Science 273(5274), 494–497 (1996).
- [8] Mehta, N., Shaik, S., Devireddy, R., and Gartia, M.R., "Single-Cell Analysis Using Hyperspectral Imaging Modalities," Journal of biomechanical engineering 140(2), 020802 (2018).
- [9] Mansfield, J.R., Gossage, K.W., Hoyt, C.C., and Levenson, R.M., "Autofluorescence removal, multiplexing, and automated analysis methods for in-vivo fluorescence imaging," Journal of biomedical optics 10(4), 041207 (2005).
- [10] Mansfield, J.R., Hoyt, C., and Levenson, R.M., "Visualization of microscopy-based spectral imaging data from multi-label tissue sections," Current Protocols in Molecular Biology 84(1), 14–19 (2008).
- [11] R Mansfield, J., "Distinguished photons: a review of in vivo spectral fluorescence imaging in small animals," Current pharmaceutical biotechnology 11(6), 628–638 (2010).
- [12] Mansfield, J., "Multispectral imaging: a review of its technical aspects and applications in anatomic pathology," Veterinary pathology 51(1), 185–210 (2014).
- [13] Malik, Z., Cabib, D., Buckwald, R., Talmi, A., Garini, Y., and Lipson, S., "Fourier transform multipixel spectroscopy for quantitative cytology," Journal of microscopy 182(2), 133–140 (1996).
- [14] Li, Q., He, X., Wang, Y., Liu, H., Xu, D., and Guo, F., "Review of spectral imaging technology in biomedical engineering: achievements and challenges," Journal of biomedical optics 18(10), 100901 (2013).
- [15] Hiraoka, Y., Shimi, T., and Haraguchi, T., "Multispectral imaging fluorescence microscopy for living cells," Cell structure and function 27(5), 367–374 (2002).
- [16] Gammon, S.T., Leevy, W.M., Gross, S., Gokel, G.W., and Piwnica-Worms, D., "Spectral unmixing of multicolored bioluminescence emitted from heterogeneous biological sources," Analytical chemistry 78(5), 1520–1527 (2006).

- [17] Keshava, N., and Mustard, J.F., "Spectral unmixing," IEEE signal processing magazine 19(1), 44–57 (2002).
- [18] Neher, R., and Neher, E., "Optimizing imaging parameters for the separation of multiple labels in a fluorescence image," Journal of microscopy 213(1), 46–62 (2004).
- [19] Favreau, P.F., Hernandez, C., Heaster, T., Alvarez, D.F., Rich, T.C., Prabhat, P., and Leavesley, S.J., "Excitation-scanning hyperspectral imaging microscope," Journal of biomedical optics 19(4), 046010–046010 (2014).
- [20] Annamdevula, N.S., Sweat, R., Griswold, J.R., Trinh, K., Hoffman, C., West, S., Deal, J., Britain, A.L., Jalink, K., et al., "Spectral imaging of FRET-based sensors reveals sustained cAMP gradients in three spatial dimensions," Cytometry Part A 93(10), 1029–1038 (2018).
- [21] Leavesley, S.J., Britain, A.L., Cichon, L.K., Nikolaev, V.O., and Rich, T.C., "Assessing FRET using spectral techniques," Cytometry Part A 83(10), 898–912 (2013).
- [22] Rich, T.C., Fagan, K.A., Nakata, H., Schaack, J., Cooper, D.M., and Karpen, J.W., "Cyclic nucleotide–gated channels colocalize with adenylyl cyclase in regions of restricted cAMP diffusion," The Journal of general physiology 116(2), 147–162 (2000).
- [23] Leavesley, S.J., Annamdevula, N., Boni, J., Stocker, S., Grant, K., Troyanovsky, B., Rich, T.C., and Alvarez, D.F., "Hyperspectral imaging microscopy for identification and quantitative analysis of fluorescently-labeled cells in highly autofluorescent tissue," Journal of Biophotonics 5(1), 67–84 (2012).
- [24] Annamdevula, N.S., Sweat, B., Favreau, P., Lindsey, A.S., Alvarez, D.F., Rich, T.C., and Leavesley, S.J., "An approach for characterizing and comparing hyperspectral microscopy systems," Sensors 13(7), 9267–9293 (2013).
- [25] Deal, J., Mayes, S., Browning, C., Hill, S., Rider, P., Boudreaux, C., Rich, T., and Leavesley, S., "Identifying molecular contributors to autofluorescence of neoplastic and normal colon sections using excitation-scanning hyperspectral imaging," Journal of biomedical optics 23(12), (2018).
- [26] Deal, J., Harris, B., Martin, W., Lall, M., Lopez, C., Rider, P., Boudreaux, C., Rich, T., and Leavesley, S.J., "Demystifying autofluorescence with excitation scanning hyperspectral imaging," presented at Imaging, Manipulation, and Analysis of Biomolecules, Cells, and Tissues XVI, 2018, 1049715.
- [27] Jain, A.K., [Fundamentals of digital image processing], Englewood Cliffs, NJ: Prentice Hall, (1989).
- [28] Mayes, S.A., Klomkaew, P., Leavesley, S.J., and Rich, T.C., "Optimization and applications of an excitation-scanning hyperspectral imaging system," presented at High-Speed Biomedical Imaging and Spectroscopy: Toward Big Data Instrumentation and Management II, 2017, 1007609.
- [29] Mayes, S.A., Leavesley, S.J., and Rich, T.C., "Excitation-scanning hyperspectral imaging system for microscopic and endoscopic applications," presented at Imaging, Manipulation, and Analysis of Biomolecules, Cells, and Tissues IX, 2016, 97110Z.
- [30] Deal, J., Favreau, P.F., Lopez, C., Lall, M., Weber, D.S., Rich, T.C., and Leavesley, S.J., "Excitation-scanning hyperspectral imaging as a means to discriminate various tissues types," presented at Imaging, Manipulation, and Analysis of Biomolecules, Cells, and Tissues XV, 2017, 1006816.

- [31] Favreau, P.F., Deal, J.A., Weber, D.S., Rich, T.C., and Leavesley, S.J., "Feasibility for detection of autofluorescent signatures in rat organs using a novel excitation-scanning hyperspectral imaging system," presented at Imaging, Manipulation, and Analysis of Biomolecules, Cells, and Tissues IX, 2016, 971113.
- [32] Leavesley, S., Jiang, Y., Patsekin, V., Rajwa, B., and Robinson, J.P., "An excitation wavelength–scanning spectral imaging system for preclinical imaging," Review of Scientific Instruments 79(2), 023707 (2008).
- [33] Leavesley, S.J., Deal, J., Hill, S., Martin, W.A., Lall, M., Lopez, C., Rider, P.F., Rich, T.C., and Boudreaux, C.W., "Colorectal cancer detection by hyperspectral imaging using fluorescence excitation scanning," presented at Optical Biopsy XVI: Toward Real-Time Spectroscopic Imaging and Diagnosis, 2018, 104890K.
- [34] Mayes, S.A., Moore, K., Browning, C., Klomkaew, P., Rich, T.C., and Leavesley, S.J., "Applications and assessment of an excitation-scanning hyperspectral imaging system," presented at Imaging, Manipulation, and Analysis of Biomolecules, Cells, and Tissues XVI, 2018, 1049706.

FIGURES

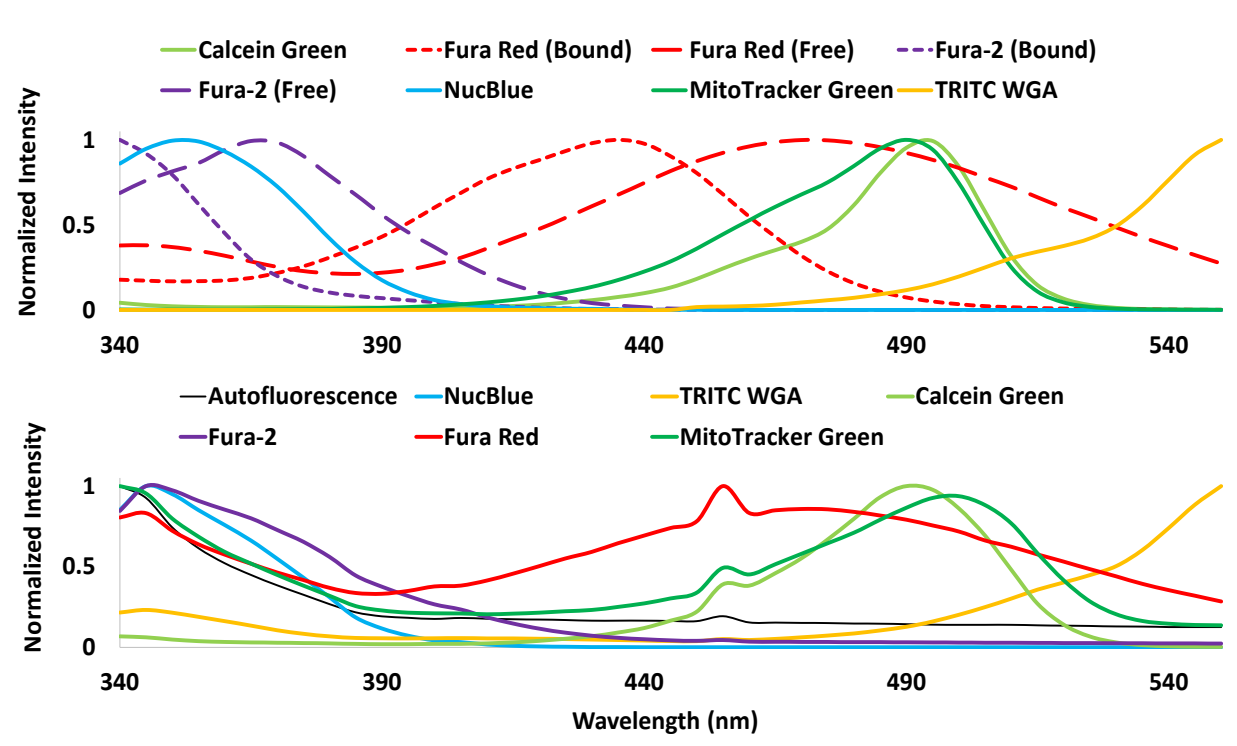


Figure 1. Libraries for excitation-scanning spectral unmixing. All values were normalized to a value of unity at the wavelength with the strongest signal. (Top) Library created from exported Thermo Fisher Scientific Spectra Viewer taken every 5 nm between 340 and 550 nm. Calcein Green (light green solid), Bound Fura Red (red short dash), Free Fura Red (red long dash), Bound Fura-2 (purple short dash), Free Fura-2 (purple long dash), NucBlue (blue solid), MitoTracker Green (green solid), and TRITC WGA (orange solid). (Bottom) Library created from single-label measurements taken on the excitation-scanning microscope every 5 nm between 340 and 550 nm. Autofluorescence (black solid), NucBlue (blue solid), TRITC WGA (orange solid), Calcein Green (light green solid), Fura-2 (purple solid), Fura Red (red solid), and MitoTracker Green (green solid).

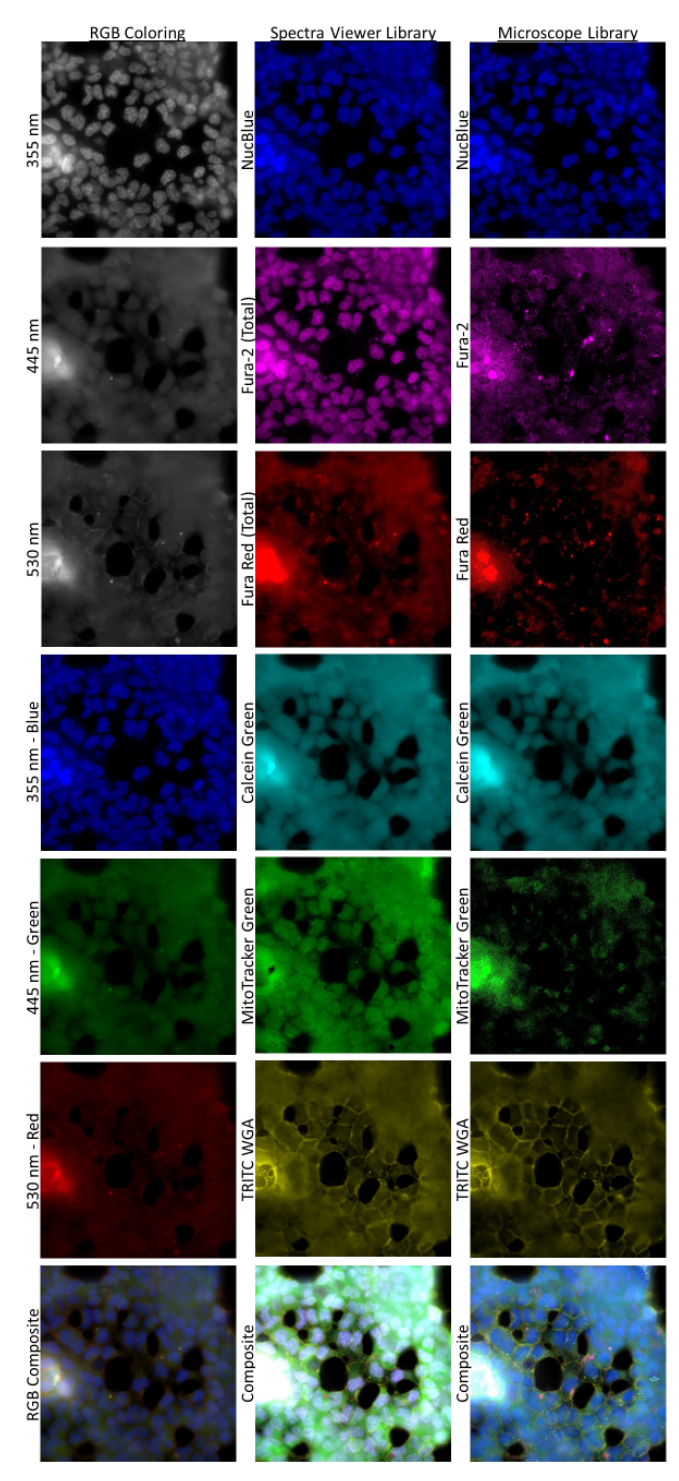


Figure 2. Comparison among visualization techniques. The left column shows the process of RGB coloring. The first three panels show the original three excitation wavelengths images chosen for false coloring, the same three images with false-color look-up tables applied, and the resultant composite image generated when the false-colored images are merged. The center column shows the component-wise false-colored results of spectral unmixing performed with the library taken from the Thermo Fisher Scientific Spectra Viewer. The right column shows the same component-wise false-colored results of spectral unmixing when performed with the library generated from the excitation-scanning spectral microscope. False color look-up tables applications for the center and right columns are as follows: blue NucBlue, magenta Fura-2, red Fura Red, cyan Calcein Green, green MitoTracker Green, yellow TRITC WGA, and an overlaid composite of these images.

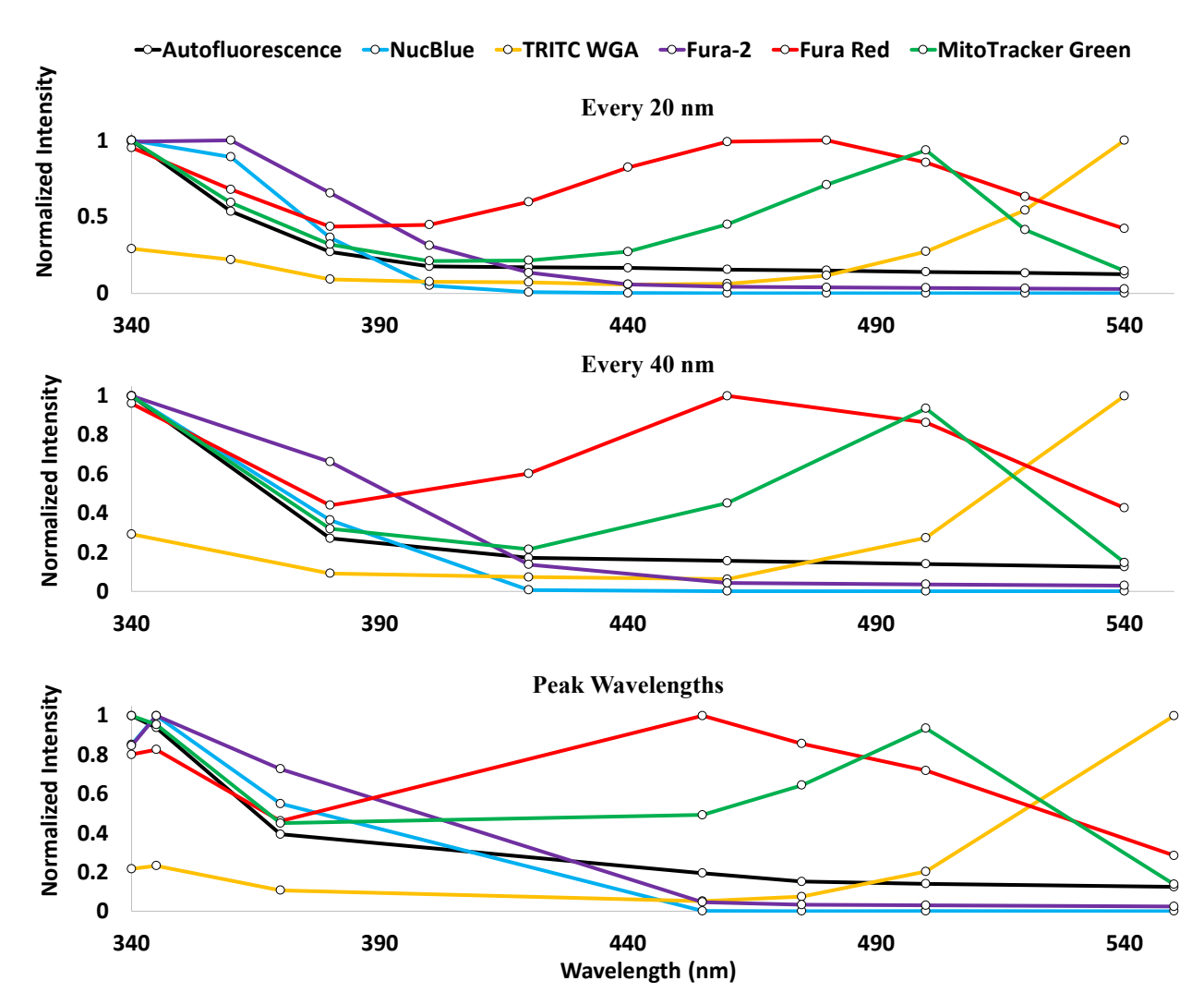


Figure 3. Libraries used for sub-selected spectral unmixing. All values were normalized to a value of unity at the wavelength with the strongest signal. The coloring is identical for all three plots: Autofluorescence (black), NucBlue (blue), TRITC WGA (orange), Fura-2 (purple), Fura Red (red), and MitoTracker Green (green). (Top) The excitation-scanning library with normalized intensity values sub-selected every 20 nm. (Middle) The excitation-scanning library with normalized intensity values sub-selected every 40 nm. (Bottom) The excitation-scanning library with normalized intensity values sub-selected to correspond to the values containing the most intense excitation wavelength per library component.

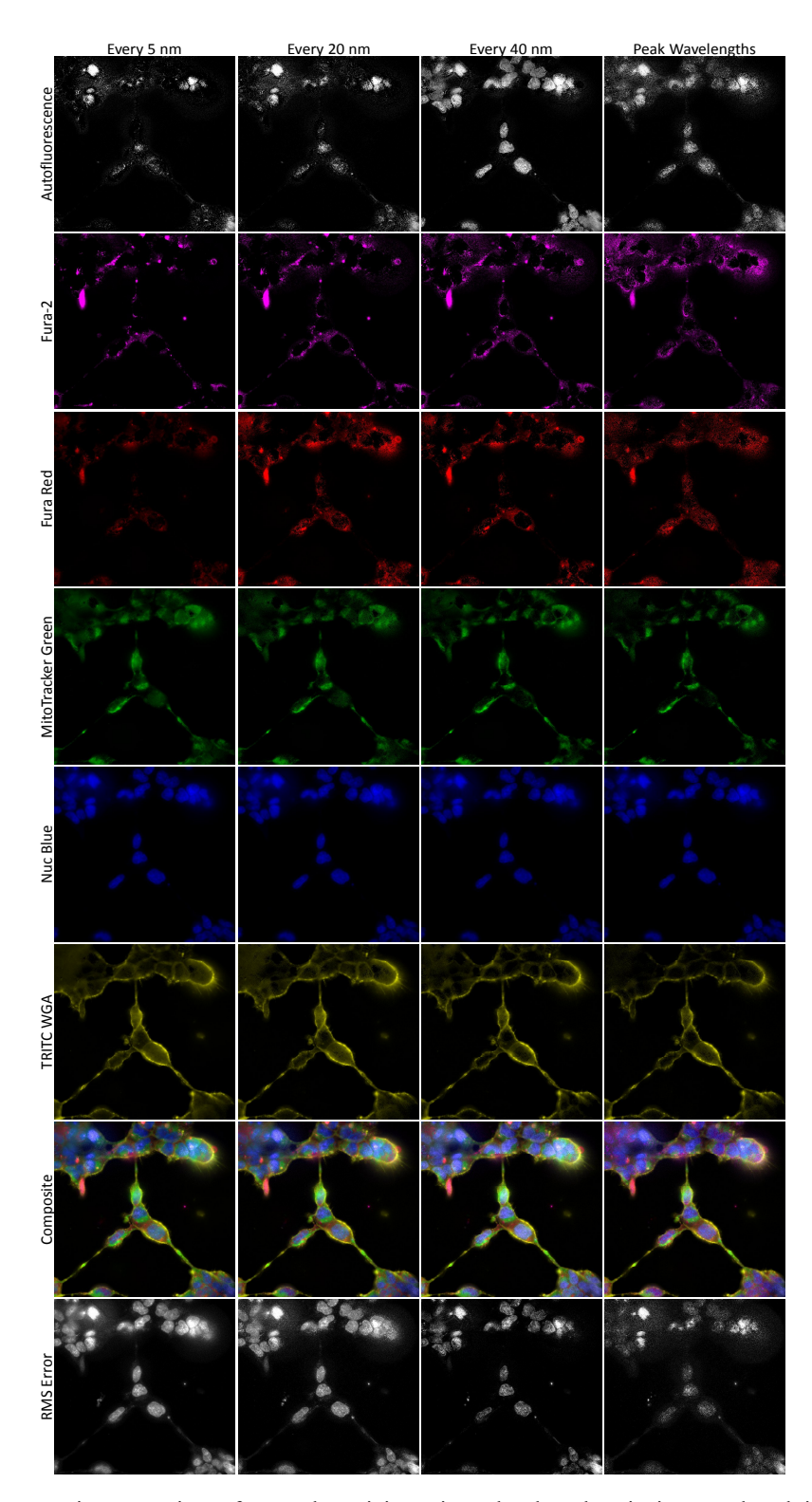


Figure 4. Component-wise comparison of spectral unmixing using sub-selected excitation wavelength images. From left to right, the columns show false-colored, unmixed images for center wavelength spacing every 5 nm, every 20 nm, every 40 nm, and specially chosen to correspond to "peak wavelengths" as described in Figure 3. From top to bottom, components include autofluorescence, Fura-2, Fura Red, MitoTracker Green, NucBlue, and TRITC WGA. The penultimate row contains the composite images generated from merging the images above them. The bottom row shows the visualized RMS error.